Robust optimisation of railway crossing geometry

Wan, Chang; Markine, Valeri; Dollevoet, Rolf

DOI
10.1080/00423114.2016.1150495

Publication date
2016

Document Version
Final published version

Published in
Vehicle System Dynamics: international journal of vehicle mechanics and mobility

VEHICLE SYSTEM DYNAMICS, 2016
VOL. 54, NO. 5, 617–637
http://dx.doi.org/10.1080/00423114.2016.1150495

Robust optimisation of railway crossing geometry

Chang Wan, Valeri Markine and Rolf Dollevoet

Section of Railway Engineering, Faculty of Civil Engineering and Geosciences, Delft University of Technology, Delft, The Netherlands

ABSTRACT

This paper presents a methodology for improving the crossing (frog) geometry through the robust optimisation approach, wherein the variability of the design parameters within a prescribed tolerance is included in the optimisation problem. Here, the crossing geometry is defined by parameterising the B-spline represented cross-sectional shape and the longitudinal height profile of the nose rail. The dynamic performance of the crossing is evaluated considering the variation of wheel profiles and track alignment. A multipoint approximation method (MAM) is applied in solving the optimisation problem of minimising the contact pressure during the wheel–rail contact and constraining the location of wheel transition at the crossing. To clarify the difference between the robust optimisation and the normal deterministic optimisation approaches, the optimisation problems are solved in both approaches. The results show that the deterministic optimum fails under slight change of the design variables; the robust optimum, however, has improved and robust performance.

ARTICLE HISTORY
Received 31 August 2015
Revised 11 December 2015
Accepted 30 January 2016

KEYWORDS
Robust optimisation; turnout crossings; rail geometry; vehicle–track interaction; track design

1. Introduction

As junctions of railway tracks, turnout crossings are weak parts of the railway network that suffer from high dynamic loads from passing trains. Studies in [1–3] show that the dynamic wheel transition over a crossing is very sensitive to changes in rail geometry and can be improved by adjusting the crossing geometry. Studies concerning numerical optimisation of the crossing geometry have been performed recently,[3,4] in which significant reduction of contact pressure and/or wear in the wheel–rail interface at a crossing has been achieved. These optimisation problems are formulated as deterministic optimisation problems, which tend to push a design towards one or more constraints until the constraints are active. For a design optimisation problem of the crossing geometry, however, uncertainties of the vehicle–track system (e.g. loading conditions and track alignment quality), as well as deviations between the theoretical design and its implementation, are inevitable. If the design variables or some system parameters cannot be achieved exactly, the deterministic

CONTACT Chang Wan c.wan@tudelft.nl, cwan0121@gmail.com

optimum (lying on one or more active constraint surfaces or the boundary of the feasible region) will fail to remain feasible.

The decision of a practical optimisation problem is often characterised by the following facts [5]:

- F.1 The optimum solution, even if computed very accurately, may be difficult to implement accurately. Moreover, deviation between a newly implemented design and a design in the service stage is inevitable;
- F.2 Uncertain disturbances, i.e. parameters that influence the evaluated properties of the solution are not deterministic in the real-world;
- F.3 The design must remain feasible for allowable (tolerated) deviations of the optimum solution;
- F.4 Optimal solutions become severely unfeasible in the face of even relatively small changes in the input parameters of the problem.

Therefore, a design optimisation problem should cope with modelling uncertainty/variability and improving or controlling performance variation. Instead of deterministic optimisation, a probabilistic formulation of the optimisation problem, which considers uncertainties, should be used.

Robust optimisation, which is one of the methods for solving a probabilistic design problem,[6] is an optimisation theory that addresses optimisation problems in which a certain measure of robustness is sought against uncertainty that can be represented as deterministic variability in the values of the parameters of the problem itself and/or its solution. That is, the optimisation process considers uncertainties in the evaluation of the objective and constraint functions. By itself, the robust optimisation methodology can be applied to every generic optimisation problem, where one can separate numerical data that can be partly uncertain and are only known to belong to a given uncertainty set from the problem's structure, which is known in advance and is common for all instances of the uncertainty problem.[7] Being designed to meet some major challenges associated with uncertainty-affected optimisation problems, the major purpose of a robust optimisation is to provide guarantees about the performance of the solution. Applications of robust optimisation in solving engineering problems can be found in many publications such as.[8–11]

In the present paper, the robust optimisation approach is proposed in the design of crossing geometry, in which the wing rails are prescribed to the selected turnout design, while the nose rail is adjusted. Based on the previous parametric study [12] on wheel transition behaviour, three design variables are chosen in the optimisation to tune the longitudinal height profile and the B-spline represented cross-sectional shape of the nose rail. The optimisation is performed with the consideration of varying wheel profiles and various track alignments. To compare with the normal deterministic optimisation approach, the optimisation problems are solved both from the deterministic optimisation and the robust optimisation approaches. Sections 2–4 clarify the criteria of crossing geometry design. The optimisation problem, formulated as deterministic optimisation and robust optimisation problems, is solved and discussed in Sections 5 and 6, respectively. Concluding remarks are provided in Section 7.

2. Wheel transition at crossings and criteria for improvement

2.1. Transition of wheel over crossing

The main source of damage to railway crossings is the dynamic impact that occurs as a wheel transfers from the wing rail to the nose rail. When impacts occur frequently at the same position, the rail can be easily broken, which is observed as one of the main damage formats of turnout crossings in the Dutch railway network. This is especially dangerous when the supporting patch of the rail/wheel contact at the impact location is small. If the wheel contacts the nose rail too close to the nose point (tip point, TP), wherein the nose rail is very thin, the contact patch will be very small. In this situation, the thin rail sustains significantly high contact pressure and is likely to be broken off. Similarly, the wing rail suffers from high contact pressure when the contact moves to the end of the wheel tread where the contact patch becomes small. Figure 1 shows the location of numerically simulated contact points on the wheel and the corresponding contact pressure when the train passes in the main-facing direction, in which it can be observed that the contact pressure becomes very high when the contact moves to the edge of the wheel tread.

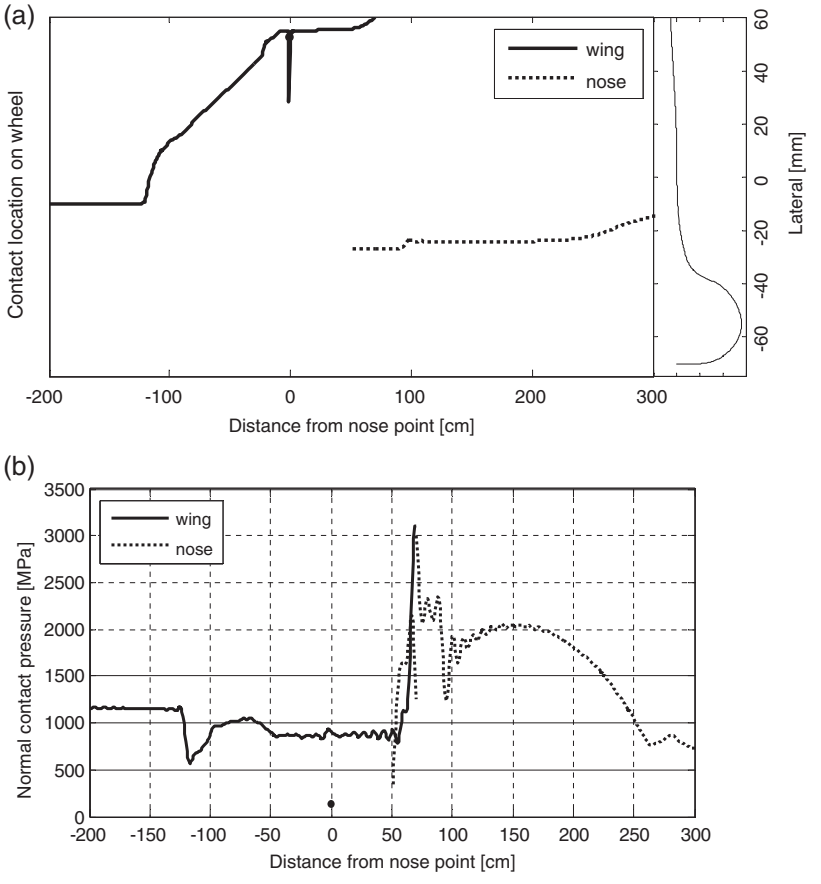

Figure 1. Dynamic response of wing rail and nose rail: (a) location of contact point on wheel, (b) contact pressure.

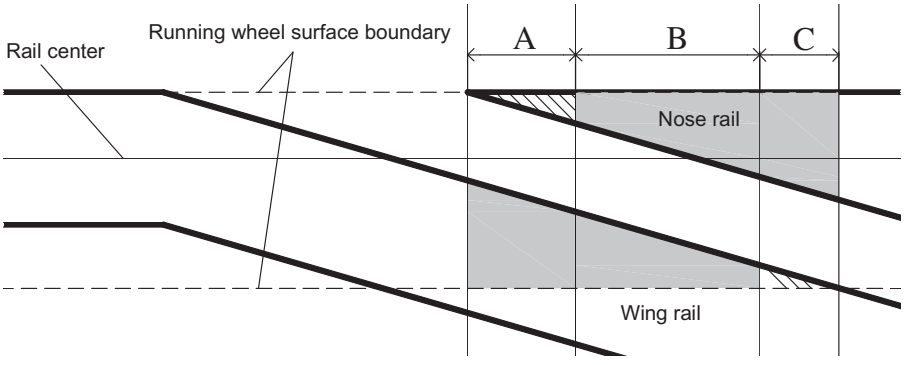

Figure 2. Transition area of a crossing—example of through route.

Therefore, to prevent severe damage to the rail and wheel, the transition of the wheel–rail contact should be neither too close to TP because the nose rail there is very thin nor too far from TP when the contact between the wheel tread edge and the wing rail is very small. A schematic illustration of the transition zone is shown in Figure 2. The wheel–rail contacts on the nose rail in zone A or on the wing rail in zone C should be avoided.

2.2. Criteria of wheel transition improvement

The impact position at the crossing nose, which indicates the location of nose rail damage, is dependent upon the crossing geometry. In [3], it was observed from the field measurements that after grinding/welding maintenance of the crossing, not only was the magnitude of impact significantly reduced but also the location of impact was shifted – leading to wider spread of impacts on the nose rail. A close look at the geometric effect on the transition location has been documented in [12], in which it is shown that both the nose rail shape and the vertical distance between the top of the wing rail and the nose rail have considerable influence on the impact location. This is especially valuable in the grinding/welding maintenance where both the reduction of impact magnitude and stress relief in the observed damaged part are demanded.

To improve the wheel transition behaviour, the study here is aimed at reducing the amplitude of dynamic impact while restraining the location of the impact through optimisation of the crossing geometry.

3. Objective vehicle–turnout system in the study

3.1. Basic vehicle–turnout system

The studied turnout is a standard one (right turn) with a curve radius of 725 m and a crossing angle of 1:15, which is the same model as in [3,12]. In the present paper, the investigations are only for a vehicle passing in the main-facing direction. The vehicle is modelled as a passenger wagon based on the VIRM (Verlengd InterRegio Materieel) passenger train,[3,12] with a static wheel load of 89 kN, the travelling speed of 140 km/h (typical speed of VIRM intercity trains in the Netherlands) and friction coefficient of 0.4 (intermediate friction level). The ‘moving track’ model from the multi-body simulation

software VI-Rail is used for modelling the dynamic vehicle–turnout interaction, in which a sampling frequency of 5000 Hz is used and the results are low-pass filtered with a cut-off frequency of 500 Hz. Note that, in the 'moving track' model, the rails and sleepers are modelled as rigid bodies moving together with wheel load and the track elasticity is independent from the location along the crossing. However, the geometry (track layout) is dependent on the longitudinal location, defined by changing rail profiles, track irregularities, extra rails (guiding rail) along the crossing. Details of the vehicle–turnout model can be found in [3,12].

3.2. Consideration of uncertain parameters

In addition to the specified parameters above, there are still uncertain parameters in the dynamic vehicle–turnout interaction, for instance, the track alignment, the quality of the fastening system and the deviation of the rail pads/ballast bed. Due to the limitation of the 'moving-track' model utilised in the study, which assumes a uniform elastic track property along the track, the variation of parameters w.r.t the track elasticity are not considered (the track elasticity parameters used in the current study can be found in Table A1 in the appendix). The following uncertain parameters are considered during the optimisation.

3.2.1. Wheel profile variation

The wheel profile plays an important role in the transition over the crossing. To investigate the dynamic vehicle–track interaction through numerical simulation, it is requested that the corresponding wheel profiles should be used. In reality, it is unwise to account for each and every wheel profile of all trains that pass through the crossing, not only because of the extremely high computational cost for thousands of simulations under various wheel profiles but also due to the inconvenience of measuring all of the wheel profiles both for different vehicles and for the same vehicles at different service cycles. Moreover, the dramatic increase in computational effort in solving the optimisation problem limits the applicability of considering many wheel profiles. Alternatively, the most representative wheel profiles among the passing trains can be used in the simulations.

In this paper two wheel profiles are selected as the representations of the wheel profiles of the passenger train VIRM in the Netherlands: the standard s1002 wheel profile (a flange height 28 mm) and the HIT wheel profile (close to a worn s1002 wheel profile after 95,000 km rolling distance) with a narrowed flange, as shown in Figure 3, in which the former is the wheel profile for new wheels and the latter is used as the re-profiling template for VIRM trains in the Netherlands. Because most VIRM trains are either equipped with new wheels (standard s1002) or regularly re-profiled as HIT profiles, it is assumed that these two wheel profiles stand for the average wheel profiles of VIRM trains.

3.2.2. Track alignment variation

Track alignment, which has significant influence on the dynamic vehicle–turnout interaction, is one of the most common control items during maintenance and manufacturing design. Here, two different track irregularities are considered: the vertical deviation of rail geometry at the crossing side, 'irr_1' (Figure 4(a)), and the lateral deviation in the rail geometry before the crossing, 'irr_2' (Figure 4(b)). The two artificial irregularities are considered in addition to the ideal track alignment to evaluate the feasibility of the crossing

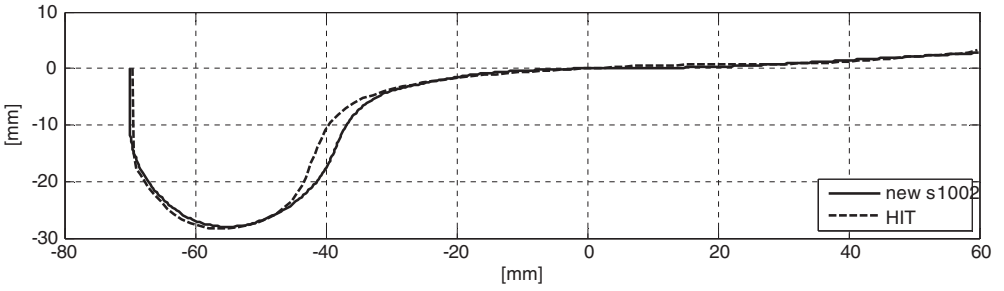

Figure 3. Representative wheel profiles of VIRM trains.

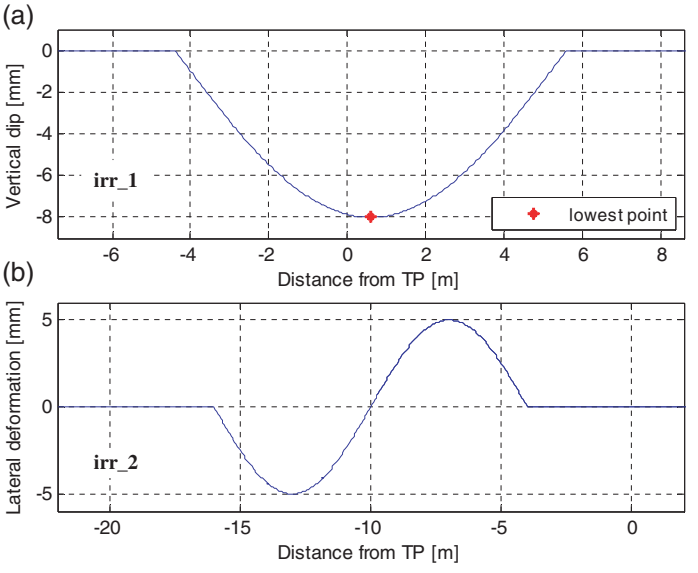

Figure 4. Track irregularities considered in crossing design: (a) vertical and (b) lateral deviation of track alignment.

geometry design, i.e. a feasible design should remain feasible under any of the three track alignments.

By including the above-mentioned uncertainties in the basic vehicle–turnout system, the problem of optimising the crossing geometry can be formulated and solved as presented in the following sections.

4. Parameterisation of crossing geometry

According to the manufacturing process of constructed crossings, the nose rail is produced by cutting/grinding the rail segments with a rail profile of the corresponding normal rail, whereas the general way of tuning the wing rail is to adjust its longitudinal height profile through a bending treatment. The results in [12] show that the vertical distance between the top of the wing rail and the nose rail affects the wheel transition behaviour. For simplicity of the problem, only the nose rail will be tuned here.

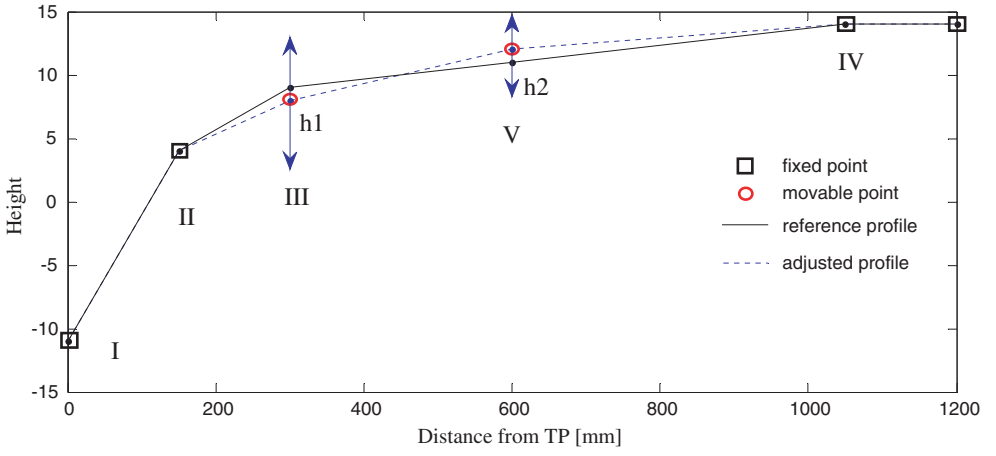

Figure 5. Longitudinal height profile of nose rail.

Definition of the crossing geometry is based on the approach used in [12], in which the nose rail is defined by five control sections along the nose rail (Figure 5) with distances of 0, 150, 300, 600 and 1050 mm from TP; the wing rail shape is fixed, using the one from the current manufacturing process. The longitudinal height profile of the nose rail is adjusted by tuning the height of the five control sections, where each height segment between two control sections is linear. It is assumed that the impact does not occur before section II where the nose rail is too thin to sustain the dynamic load. Thus, only the heights of sections III and V are to be tuned. The longitudinal height profile of the nose rail is shown in Figure 5, in which the height of 0 mm is set to 14 mm below the top of the normal rail. When tuning the height profile, the monotonic increase in the profile is maintained to obtain a realistic design. The heights of the control cross-sections III and V are defined by parameters h and t.

$$h_1 = h, \quad h_2 = h + t.$$

The shape of the nose rail is defined using a cubic B-spline, in which six control points are used as shown in Figure 6. The parametric in [12] shows that the control point P_3 has a major influence on the dynamic transition behaviour of the wheel, whereas the remaining control points are less affective. Therefore, P_3 is set as a movable control point along the line PM to adjust the transverse shape of the nose rail. The position of P_3 is defined by the parameter λ: $\lambda = |PP_3/PM|$. A positive λ means P_3 locates inside the segment PM, and a negative λ indicates that P_3 moves to the other side of P (outside the segment PM).

Thus, the crossing geometry here is defined by the three parameters: h, t and λ.

5. Deterministic optimisation problem

The multipoint approximation method (MAM),[13–15] which has been applied in the design optimisation of railway tracks,[3,16,17] is used to solve the crossing geometry optimisation problem. Firstly, the deterministic optimisation problem is to be solved without considering the tolerance of design variables.

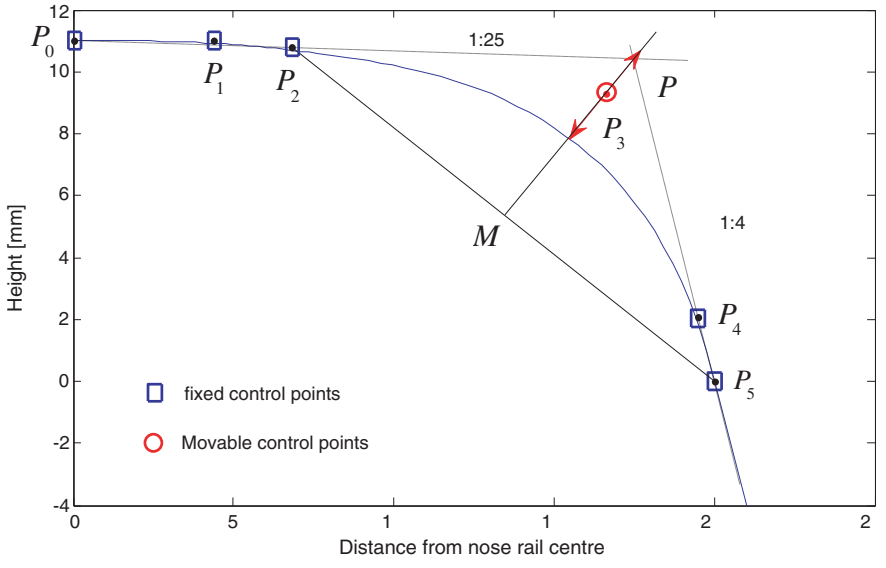

Figure 6. B-spline representation of nose rail profile (symmetric).

5.1. Formulation of deterministic optimisation problem

A general optimisation problem can be stated in the following form:
Minimise

$$F_0(\boldsymbol{x}) \rightarrow \min, \quad \boldsymbol{x} \in R^N \tag{1}$$

subject to

$$g_j(\boldsymbol{x}) \leq 1, \quad j = 1, \ldots, M \tag{2}$$

and

$$A_i \leq x_i \leq B_i, \quad i = 1, \ldots, N, \tag{3}$$

where F_0 is the objective function; g_j is the constraint; $\boldsymbol{x}$ is the vector of design variables; A_i and B_i are the side limits which define the lower and upper bounds of the ith design variable.

5.1.1. Design variables

The design variables of the optimisation problem are the adjusting parameters of the crossing geometry, as introduced in Section 4.

$$\boldsymbol{x} = [h, t, \lambda] \tag{4}$$

with:

$$\begin{aligned} &5 \leq h \leq 14(\text{mm}), \\ &0 \leq t \leq 6(\text{mm}), \\ &-1/5 \leq \lambda \leq 1. \end{aligned} \tag{5}$$

The reference design is $\boldsymbol{x}_{\text{ref}} = [9,\ 2,\ 1/3]$. Dynamic vehicle–track interaction will be analysed for each of the two different wheel profiles shown in Figure 3.

5.1.2. Objective function

The objective function is formulated based on Equation (6), in which the contact pressure (S) and wear number (W) are to be minimised:

$$F_0(\boldsymbol{x}) \equiv w_1 \sum_{i=1}^{d} \alpha_i \frac{\bar{S}_i(\boldsymbol{x})}{\bar{S}_i^*} + w_2 \sum_{i=1}^{d} \alpha_i \frac{\bar{W}_i(\boldsymbol{x})}{\bar{W}_i^*} \rightarrow \min, \tag{6}$$

where d is the total number of wheel profiles evaluated in the optimisation problem. α_i is the weight coefficient for the ith wheel profile, $\sum_{i=1}^{d} \alpha_i = 1$. In the present paper, two different wheel profiles are considered; thus, d equals 2. Considering the fact that the HIT wheel profile (second wheel) is more commonly used than the standard s1002 wheel profile (first wheel), the HIT wheel is given more weight. The weight coefficient pair $[\alpha_1,\ \alpha_2] = [0.25,\ 0.75]$ is applied. $\bar{S}_i$ and $\bar{W}_i$ are the accumulative contact pressure and wear number on the crossing, respectively, and are expressed in the form of the Kresselmeier–Steinhauser function (KS function).[3]

$$\bar{S}(\boldsymbol{x}) = \frac{1}{\mu} \ln \left[\sum_{i=1}^{T} e^{\mu S(\boldsymbol{x}, t_i)/S_{\max}(\boldsymbol{x})} \right] \cdot S_{\max}(\boldsymbol{x}), \tag{7}$$

$$\bar{W}(\boldsymbol{x}) = \frac{1}{\mu} \ln \left[\sum_{i=1}^{T} e^{\mu W(\boldsymbol{x}, t_i)/W_{\max}(\boldsymbol{x})} \right] \cdot W_{\max}(\boldsymbol{x}), \tag{8}$$

where

$$S_{\max}(\boldsymbol{x}) = \max(S(\boldsymbol{x}, t_i)), \quad i = 1,\ \ldots, T,$$
$$W_{\max}(\boldsymbol{x}) = \max(W(\boldsymbol{x}, t_i)), \quad i = 1, \ldots, T,$$

Here, T is the total number of time points during the simulations. The parameter μ determines the discrepancy between $\bar{S}(\bar{W})$ and the most critical value $S_{\max}(W_{\max})$. In the present paper, μ equal to 50 is used in all KS functions. A more detailed explanation of the KS formation of the objective can be found in [18,19]. The normalising factors $\bar{S}_i^*$ and $\bar{W}_i^*$ from Equations (7) and (8) are the cumulative contact pressure and wear number, respectively, of the reference design corresponding to the ith wheel profile.

w_1 and w_2 are the weight coefficients for contact pressure and wear, respectively, $w_1 + w_2 = 1$. For the sake of simplicity, the evaluation of wear number is ignored in this optimisation problem (i.e. $w_2 = 0$). It should be noted that during the optimisation the contact pressure at each time point refers to the largest contact pressure from all of the contact points in the case of multipoint contact.

5.1.3. Constraints

Several constraints on the dynamic response of the wheel transition behaviour are defined in the optimisation problem.

Geometric constraints: g_geo

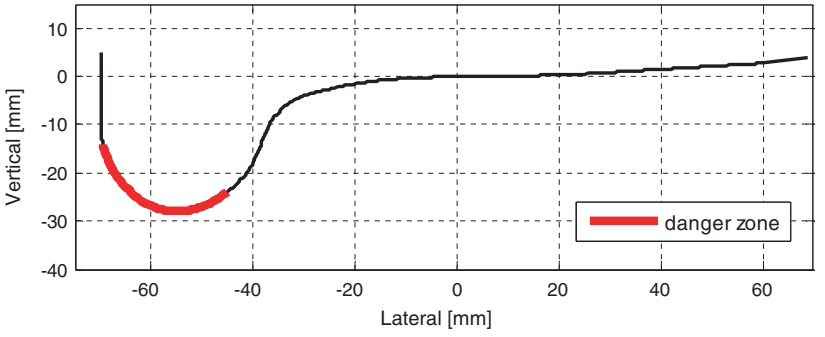

Figure 7. 'Danger zone' of wheel–rail contact on wheel.

Constraints on the geometric shape of the nose rail are considered in the problem. In addition to the side limits of the design variables, additional restrictions are posed on the longitudinal height profile of the nose rail and the cross-sectional shape of the nose rail.

On the one hand, the height of the nose rail should be monotonically increased between cross-sections I and IV, and the maximum height of the nose rail should not exceed 14 mm. On the other hand, the spline-represented nose rail shape described by a set of points with $y-z$ coordinates should be a smooth convex curve (Figure 6), which requires the curvature of the profile at any segment (defined by three adjacent points) to be no larger than zero. Here, the curvature sign of the ith segment of the nose rail profile for design vector $\boldsymbol{x}$ is defined as

$$cv_i = (\boldsymbol{p}_{i+1} - \boldsymbol{p}_i) \cdot (\boldsymbol{p}_i - \boldsymbol{p}_{i-1}), \quad i = 2, \ldots, n-1, \tag{9}$$

where $\boldsymbol{p}_i$ is the coordinates of the ith point (the first point starts from the top of the nose rail centre) of the nose rail profile and n is the total number of points. The constraint of the profile convexity is expressed as

$$g_{cv} \equiv \sum_{i=2}^{n-1} \max[cv_i(\boldsymbol{x}),\ 0] \leq 0. \tag{10}$$

Constraint on impact location: g_iml. The transition of passing wheels is restrained in the allowed area as discussed in Section 2, that is, the wheel–rail contact should not occur in zone A and zone C (Figure 1). In this paper, zone A is defined as 0–250 mm from TP on the nose rail and zone C starts from 650 mm away from TP on the wing rail.

Constraint on derailment: g_drm. To avoid derailment, a constraint is imposed on the position of the contact point w.r.t the wheel. The danger zone of wheel–rail contact is assumed as 45 mm away from the nominal centre (where the wheel radius equals to the nominal wheel radius) of the wheel towards the flange back side, as shown in Figure 7. Wheel–rail contact in the danger zone is indicated as a wheel climbing over the rail, which will consequently result in derailment. Therefore, wheel–rail contact should not occur in the danger zone. As an exception, the wheel flange back contact on the guard rail is not recognised as a derailment risk.

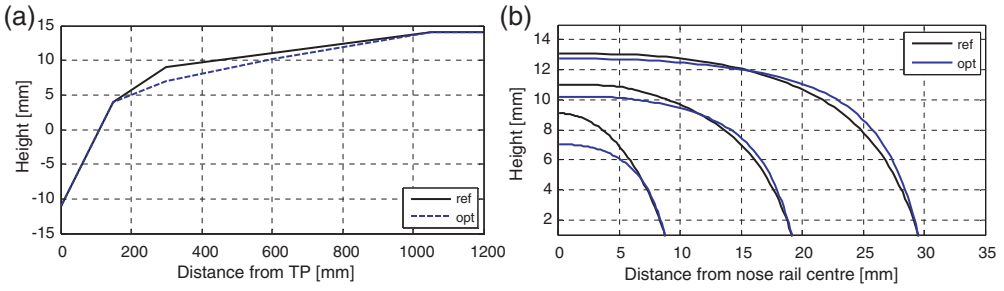

Figure 8. Comparison of crossing geometry between deterministic optimum (opt) and reference design (ref): (a) longitudinal height profile of nose rail, (b) changing nose rail shape at locations 300, 600 and 900 mm away from TP.

It should be noted that the constraint g_geo is evaluated without dynamic simulations, whereas the constraints g_iml and g_drm are investigated based on the dynamic response of the crossing under the ideal track alignment and the track alignments irr_1 and irr_2 (Section 3.2.2). The constraints are formulated as

$$\begin{aligned} g\_\text{geo} &\equiv g\_\text{geo}(\boldsymbol{x}) \leq 1, \\ g\_\text{iml} &\equiv \max(g\_\text{iml}_j(\boldsymbol{x})) \leq 1, \quad j = 1, 2, 3, \\ g\_\text{drm} &\equiv \max(g\_\text{drm}_j(\boldsymbol{x})) \leq 1, \quad j = 1, 2, 3. \end{aligned} \tag{11}$$

Here, j refers to the condition of the track alignment: $j = 1$, ideal track alignment; $j = 2$, track alignment irr_1; and $j = 3$, track alignment irr_2.

Therefore, the deterministic optimisation problem formulated using functions (6) and (11) with the design vector described in Equations (4) and (5) can be solved.

5.2. Results of deterministic optimisation problem

Similar to many common optimisation tools, MAM is not a global optimisation method that can guarantee a solution to be the global minimum in a nonlinear programming problem. To obtain a solution as close to the global optimum as possible, the optimisation problem is solved with various initial points, among which the solution (feasible) with the minimum objective value is selected as the optimum.

5.2.1. Optimal solution from deterministic optimisation

The optimum design of the deterministic optimisation problem (deterministic optimum) is obtained as $[h,\ t,\ \lambda] = [7.030,\ 3.186,\ 0.155]$. A comparison of the optimum design and the reference design is shown in Figure 8, wherein it can be seen that the nose rail is lower than that of the reference design; the cross-sectional shape of the nose rail is changed as well, wherein the gauge corner has moved outwards.

It is interesting to note that in a previous study,[3] the nose rail was raised up for the design with minimisation of only the contact pressure, as shown in Figure 9. To understand the difference, the contact pressure of the current optimum design is presented in Figure 10. In this design, the impact occurs at approximately 500 mm away from TP (location of maximum contact pressure), where the vertical distance between the top of the wing

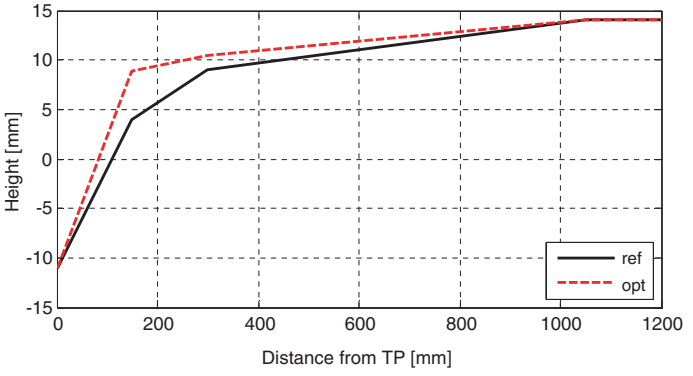

Figure 9. Longitudinal height profile of crossing nose (ref: reference design, opt: optimal solution from previous study [3]).

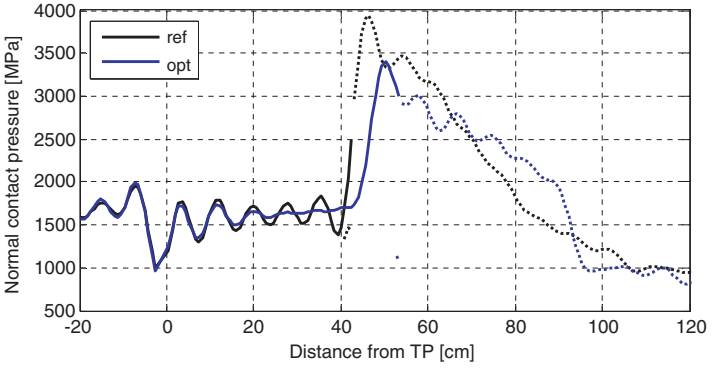

Figure 10. Contact pressure w.r.t distance from TP (ref: reference design, opt: deterministic optimum).

rail and the nose rail is 4.82 mm. In the previous study, the impact was located approximately 205 mm away from TP, and the vertical distance between the top of the wing rail and the nose rail was 4.63 mm, which is very close to the optimal design obtained here. This indicates that the vertical distance between the top of the wing rail and the nose rail at the transition zone, especially the transition point, is a key factor that influences the dynamic behaviour of a crossing.

The reason why the two optimisations result in designs with different impact locations can be explained by the fact that the current study has a constraint on the transition location (250–650 mm away from TP) and thus the impact location is restricted; however, no constraint of impact location was imposed in the former study. Moreover, the track alignments used for calculating the objective function are different in the two studies: track alignment irr_1 was used in [3], and the ideal track alignment is used here.

To minimise the contact pressure due to impact, the longitudinal height profile of the crossing rails is, however, not the unique parameter that determines the impact location. An optimised solution is obtained as a result of the longitudinal height profile and the cross-sectional shape of the nose rail.

Table 1. Parameters and level settings in the full-factorial design.

Factors	Parameter description	Level 1	Level 2	Level 3
x1	Variation of cross-sectional shape of the nose rail w.r.t the design parameter λ: $\Delta\lambda$	-0.01	0	0.01
x2	Variation of longitudinal height profile of the nose rail w.r.t the design parameters [h, t]: [Δh, Δt]	$[-0.1, -0.1]$	[0, 0]	[0.1, 0.1]

Table 2. Design variances.

	Level of factors	
Design variance	**x1**	**x2**
v1	1	1
v2	2	1
v3	3	1
v4	1	2
v5	2	2
v6	3	2
v7	1	3
v8	2	3
v9	3	3

5.2.2. Assessment of deterministic optimal solution under design uncertainties

In the manufacturing process and the grinding/welding maintenance of the crossings, a deviation between the theoretical design and the implementation is inevitable. Thus, a further evaluation of the dynamic crossing performance that accounts for the design uncertainties is important.

A three-level, full-factorial design of experiments (DOE) is applied for sampling the variations of the design variables with a given tolerance. Table 1 shows the parameters and level settings of the DOE, in which the variation of the longitudinal height profile of the nose rail is simplified as a combined parameter to reduce the sampling size. A relatively large tolerance (± 0.1 mm) of the longitudinal height profile (**x2**) is considered in the level setting, corresponding to the tolerance during the manual grinding/welding maintenance of crossings. In total, there are $3^2 = 9$ design variances, i.e. variances of the design vector, as listed in Table 2.

The feasibility and the robustness of the design as a result of applying the design variances is checked. Here, the constraints on the impact location (g_iml) and on the derailment (g_drm) that are expressed in Equation (11) are used to evaluate the design feasibility. Table 3 shows the results of the objective value and the feasibility evaluation of the design under each design variance, in which it can be observed that the constraint on derailment is violated under variance v1 and v4; therefore, the design becomes unfeasible. Moreover, the objective values of the unfeasible designs are much higher, which results in increasing the relative standard deviation (RSD) of the sampling objective values.

These results indicate that the optimum design from the deterministic optimisation failed with slight variation of the design vector. Therefore, a probabilistic optimisation approach should be applied to deal with the uncertainty of design parameters in the optimisation problem.

Table 3. Results of feasibility and robustness analysis (deterministic optimum).

Design variance	Objective value	*g*_iml	*g*_drm	feasibility
v1	1.295	0.8323	1.4123	infeasible
v2	0.792	0.8084	0.5294	feasible
v3	0.777	0.7964	0.5270	feasible
v4	1.294	0.8323	1.4173	infeasible
v5	0.738	0.7964	0.5218	feasible
v6	0.780	0.7964	0.5243	feasible
v7	0.794	0.8323	0.5243	feasible
v8	0.740	0.8203	0.5246	feasible
v9	0.783	0.7964	0.5218	feasible
RSD of objective value: 0.260306				

Notes: The constraint values of *g*_iml and *g*_drm here are chosen as the maximum values among the sub-constraint functions of *g*_iml and *g*_drm, respectively. A constraint value larger than 1 means this constraint is violated.

6. Robust optimisation problem

6.1. Formulation of robust optimisation problem

A robust optimisation approach is formulated based on the deterministic optimisation problem to cope with the deviation of the design in the implementation process.

6.1.1. General formulation of robust optimisation problem

A generic robust optimisation problem can be expressed as in [20]:

Minimise

$$F_0(\boldsymbol{x}, \boldsymbol{\xi}), \quad \boldsymbol{x} \in R^N, \boldsymbol{\xi} \in R^k \tag{12}$$

subject to

$$g_j(\boldsymbol{x}, \boldsymbol{\xi}) \leq 1, \quad j = 1, \ldots, M \tag{13}$$

and

$$A_i \leq x_i \leq B_i, \quad i = 1, \ldots, N, \tag{14}$$

where the design vector $\boldsymbol{x}$, constraints $g(\boldsymbol{x})$, and the objective function $F_0(\boldsymbol{x})$ are all of the same as those in the deterministic optimisation problem. The parameter $\boldsymbol{\xi}$ stands for the disturbance vectors or parameter uncertainties, which in this study is the variation of the design vector.

6.1.2. Objective function

Different from reliability-based approaches that focus on the probability of constraint satisfaction or violation,[21,22] a robust design method emphasises primarily the level of performance variation, i.e. the sensitivity of the design.[6,7,23] In a robust optimisation problem, a design with maximum/minimum 'mean on target' and 'minimised variance' under uncertainties is sought for. Basically, the variance of the structural performance can be roughly described by its standard deviation (SD) or RSD. Therefore, a robust

optimisation problem is generally formulated as a multi-objective problem:

$$F_0^{\mathrm{rbs}}(\boldsymbol{x},\boldsymbol{\xi}) \equiv [\mu(F_0(\boldsymbol{x},\boldsymbol{\xi})),\sigma(F_0(\boldsymbol{x},\boldsymbol{\xi}))] \rightarrow \min, \tag{15}$$

$\mu(F_0(\boldsymbol{x},\boldsymbol{\xi}))$ is the mean value of the stochastic response $F_0(\boldsymbol{x},\ \boldsymbol{\xi})$ and $\sigma(F_0(\boldsymbol{x},\ \boldsymbol{\xi}))$ is the variance of the response $F_0(\boldsymbol{x},\ \boldsymbol{\xi})$. A common approach for solving this problem is to use a weighted-sum objective function $\bar{F}_0^{\mathrm{rbs}}(\boldsymbol{x},\ \boldsymbol{\xi})$:

$$\bar{F}_0^{\mathrm{rbs}}(\boldsymbol{x},\boldsymbol{\xi}) = \alpha\frac{\mu(F_0(\boldsymbol{x},\boldsymbol{\xi}))}{\hat{\mu}} + (1-\alpha)\frac{\sigma(F_0(\boldsymbol{x},\boldsymbol{\xi}))}{\hat{\sigma}} \rightarrow \min, \tag{16}$$

where $\alpha \in (0,\ \ 1)$ is the weight of the mean and $1-\alpha$ is the weight of the variance of the response; $\hat{\mu}$ and $\hat{\sigma}$, which are used as normalising factors, are the mean and the variance of the response of the reference design, respectively.

In this study the formulation of the robust optimisation problem is adjusted in consideration of the following:

- It is difficult to choose proper weights for the mean and variance of the objective value.
- A weighted-sum formulation has the risk of increasing one of the objectives.

To gain the minimum mean response and to maintain the robustness of the response, a single-objective formulation that considers only the mean response ($\alpha = 1$) is adopted, as shown in Equation (17). Meanwhile, the variance (RSD) of response $F_0(\boldsymbol{x},\ \boldsymbol{\xi})$ is treated as a constraint (g_{rsd}).

$$\bar{F}_0^{\mathrm{rbs}}(\boldsymbol{x},\boldsymbol{\xi}) = \frac{\mu(F_0(\boldsymbol{x},\boldsymbol{\xi}))}{\hat{\mu}} \rightarrow \min, \tag{17}$$

$$g_{\mathrm{rsd}}(\boldsymbol{x},\boldsymbol{\xi}) = \sigma(F_0(\boldsymbol{x},\boldsymbol{\xi}))/0.05 \leq 1, \tag{18}$$

That is, the RSD should not be larger than 0.05 so that the stochastic response of the optimum solution can be assured with a confidence level of no less than 90%.

6.1.3. Constraints

A common formulation of the constraint function is shown in Equation (13), where all of the constraints are calculated considering variation of the design vector. Moreover, a robust solution should have a minimised SD of the response both for the objective value and for the constraint values. In this study, however, the constraints are treated in an adjusted format.

Firstly, minimisation of the variance of constraints is not required when applying design variances. That is, no extra constraints are imposed on the basic constraints as in the case of the objective function (Equation (18)). In this way, the focus of robustness is on the objective values.

Secondly, the satisfaction/violation of constraints under design variances is not evaluated for all constraints. Here, the constraints *g*_iml and *g*_drm are assessed for each design variance, whereas the constraint *g*_geo is assessed only for the original design vector at each search point. Therefore, a tolerance of the geometry is allowed if all constraints are satisfied for the original design. The feasibility of a design is then driven by the satisfaction

of the constraints g_iml and g_drm obtained from the dynamic behaviour of the crossing under design variances. Thus, a constraint is defined by the worst response from the design variances, that is, the one most violated or closest to violation among all design variances.

The constraints of the robust optimisation problem are adjusted as

$$\begin{aligned} g_{\text{geo}} &\equiv g_{\text{geo}}(\boldsymbol{x}) \leq 1, \\ g_{\text{iml}} &\equiv \max(g_{\text{iml}}(\boldsymbol{x}, \boldsymbol{\xi})) \leq 1, \\ g_{\text{drm}} &\equiv \max(g_{\text{drm}}(\boldsymbol{x}, \boldsymbol{\xi})) \leq 1, \\ g_{\text{rsd}}(\boldsymbol{x}, \boldsymbol{\xi}) &= \sigma(F_0(\boldsymbol{x}, \boldsymbol{\xi}))/0.05 \leq 1. \end{aligned} \tag{19}$$

Therefore, the robust optimisation problem formulated using functions (17) and (19) with the design vector in Equations (4) and (5) can be solved. Now it is in the general form Equations (12) and (14) and any method for solving nonlinear programming problems can be used.

6.2. Robustness evaluation

It is assumed that a design obtained from the robust optimisation should remain feasible and improved with a meaningful variation of the design vector. To evaluate the robustness of a design, the constraints and objective values must be estimated for all variations of the design vector during optimisation. Consequently, robust optimisation can become prohibitively expensive. Instead of infinite variations, sampling methods can be used to measure the possible parameter variations, through which the size of estimation points can be defined. In this study, the design variances from Tables 1 and 2, which are sampled using the DOE method, are used to represent the uncertainty of the design vector in the robust optimisation problem.

6.2.1. Modified robustness evaluation approach

In principle, the robustness of each design should be evaluated by assessing the design under all design variances. To reduce the calculation time of the robust optimisation, a computationally cheaper approach is applied by performing a selective robustness evaluation. Once the design becomes unfeasible under one design variance, the robustness analysis of the design is stopped. Therefore, the objective value in Equation (17) and constraint values in Equation (19) are calculated based on the evaluated design variances in the robustness analysis, which may not include all nine variances listed in Tables 1 and 2.

6.2.2. Extra penalty for unfeasible design without applying design variance

Before applying design variances, the feasibility of the design from the current search point is checked. It is suggested that a design that becomes unfeasible before applying design variances is farther beyond the feasible area than a design that becomes unfeasible after assigning design variances. Because the objective and constraint values are obtained from the evaluated design variances, in the case of a sampling size equal to one, the RSD of the objective value will be zero. Hence, the constraint g_{rsd} is always satisfied. Although the design is unfeasible, the severance of infeasibility may not be recognised among other

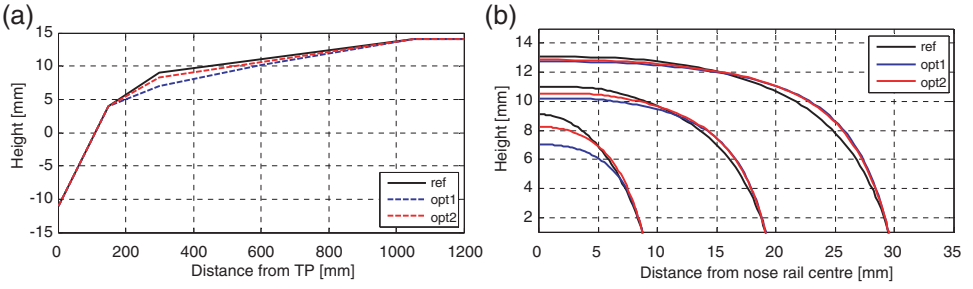

Figure 11. Comparison of crossing geometry between the optimum solutions (opt1: deterministic optimum, opt2: robust optimum) and reference design (ref): (a) longitudinal height profile of nose rail, (b) changing nose rail shape at locations 300, 600 and 900 mm away from TP.

search points that become unfeasible after assigning design variances apart from the original design. To cope with this situation, an extra penalty to the RSD is proposed if the design is unfeasible without applying design variances.

A new RSD is defined based on the violated constraints expressed as

$$\sigma(F_0(\boldsymbol{x})) = 0.05 + \sum_{j=1}^{M} k_p \cdot \max[g_j(\boldsymbol{x}) - 1, 0], \tag{20}$$

where M is the total number of constraint functions defined in Equation (11); $g_j(\boldsymbol{x})-1>0$ indicates that the constraint is violated; k_p is the penalty factor for RSD, which, in this study, is taken as $k_p = 10^2$. Therefore, a high RSD will be obtained, which consequently results in severe violation of the constraint g_{rsd}.

6.3. Results of optimisations

The robust optimisation problem is solved using various initial points, among which the solution (feasible) with minimum objective value is selected as the optimum.

6.3.1. Optimal solution from robust optimisation

The optimum design from the robust optimisation (robust optimum) is obtained as $[h,\ t,\ \lambda] = [8.250,\ 2.300,\ 0.186]$. A comparison of the reference design and the optimum designs from both the deterministic optimisation and the robust optimisation is shown in Figure 11, wherein it can be observed that the nose rail of the robust optimum is higher than that of the deterministic optimum and lower than that of the reference design.

6.3.2. Robustness of optimum solution

Table 4 shows the results of the objective value and the feasibility of the design under each design variance considered during the optimisation, indicating that the optimum solution from the robust optimisation is robust and the design remains reliable under all design variances.

The results of the dynamic wheel transition behaviour, including the response under each design variance estimated during the robust optimisation, are shown in Figure 12, wherein the results of the robust optimum and the reference design are marked with 'opt'

Table 4. Results of feasibility and robustness analysis (robust optimum).

Design variance	Objective value	*g*_iml	*g*_drm	feasibility
v1	0.716	0.7965	0.5266	feasible
v2	0.739	0.7965	0.5276	feasible
v3	0.775	0.7965	0.5292	feasible
v4	0.719	0.7965	0.5243	feasible
v5	0.743	0.7965	0.5251	feasible
v6	0.773	0.7965	0.5271	feasible
v7	0.732	0.7965	0.5221	feasible
v8	0.751	0.7965	0.5233	feasible
v9	0.780	0.7965	0.5251	feasible
RSD of objective value: 0.032300				

Notes: The constraint values of *g*_iml and *g*_drm here are chosen as the maximum values among the sub-constraint functions of *g*_iml and *g*_drm, respectively. A constraint value larger than 1 means this constraint is violated.

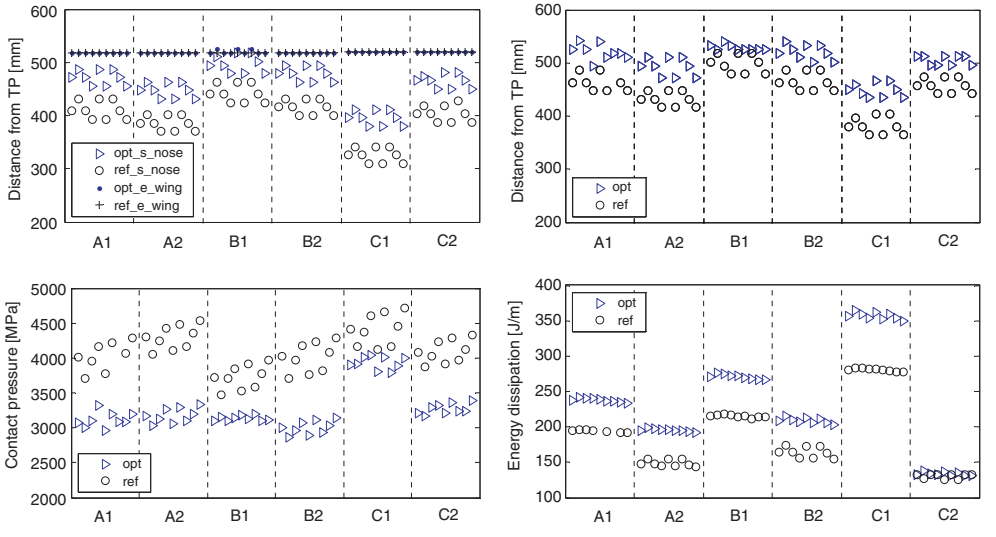

Figure 12. Results of the robust optimum crossing design: (a) Location of wheel transition (s_nose: start location of the contact on nose rail, e_wing: end location of the contact on wing rail), (b) location of impact on nose rail, (c) accumulative contact pressure, and (d) Accumulative energy dissipation.

Table 5. Variations of the vehicle–turnout system.

Variations	Wheel profile	Track alignment
A1	s1002	ideal alignment
A2	HIT	ideal alignment
B1	s1002	with vertical irregularity irr_1
B2	HIT	with vertical irregularity irr_1
C1	s1002	with lateral irregularity irr_2
C2	HIT	with lateral irregularity irr_2

and 'ref', respectively. To clarify the results, the comparison is performed in six groups classified by two variations of the wheel profiles and three variations of the track alignment, as listed in Table 5.

The core part of the wheel transition zone (zone B in Figure 2), i.e. from the location of the start of contact on the nose rail to the end of contact on the wing rail, is shown in Figure 12(a). It can be observed that the first contact on the nose rail has been shifted farther from TP compared with the reference design, whereas the location of the last contact on the wing rail has little change.

Figure 12(b) shows the impact location defined by the location of the maximum contact pressure, wherein the impact location is altered to be farther from TP, which indicates that the potential damage location moves further away. Because the thickness of the nose rail increases gradually from TP, the farther the impact on the nose rail is, the less the damage at the crossing will be.

Figure 12(c) compares the accumulated contact pressure (Equation (8)) between the reference design and the robust optimum, in which significant reduction of the contact pressure is recognised. It should be mentioned that the upper limit of the Y-axis has been fixed at 5000 MPa, which covers the results under all of the design variances of the optimum design and most design variances of the reference design. The results of the reference design under some design variances that have much higher contact pressure are not visible in this figure. In other words, the reference design is not robust according to the evaluations in this study. The optimum design, however, has robust behaviour, as shown in Figure 12(c).

The above results show that the design from the robust optimisation has robust and improved performance under the ideal track alignment and the existence of irregularities, both for the nominal s1002 wheel profile and for the HIT profile. Regarding the wheel profiles, the improvement of the transition behaviour is more significant under the HIT wheel profile which has been weighted more in the objective function. Moreover, it is observed that the wheel transition behaviour differs under various track alignments. Among the three cases of track alignment, the lateral serpentine deformation of the rail (groups C1 and C2) has more negative influence on the wheel transition behaviour, which indicates that the occurrence of this type of track alignment is more risky for crossings.

Note that, because the reduction of the energy dissipation at the wheel–rail contact patch is excluded in the robust optimisation problem, an increase in the energy dissipation is obtained as shown in Figure 12(d), which raises the risk of wear damage at the crossing. Therefore, the optimisation problem can be adjusted to take into account the attenuation of wear.

7. Conclusion

This paper presents a methodology for improving wheel transition behaviour by tuning the crossing geometry through a robust optimisation approach, in which the variations of wheel profiles and track alignments have been accounted for. The wheel transition behaviour is evaluated based on the contact pressure at the wheel–rail interface and the location of the wheel transition from the wing rail to the nose rail. If the transition locates within the defined safe area, then the lower the contact pressure is, the better the wheel transition behaviour will be. Compared with the current manufacturing design, the optimum design results in lower height profile and a wider, flatter cross-sectional shape of the nose rail.

To clarify the difference between a normal deterministic optimisation approach and a robust optimisation approach, the problem is solved using both the deterministic and robust optimisation methods. The deterministic optimal solution results in better objective value, although it fails under slight change of the design vector. The optimal solution from the robust optimisation, however, has robust performance with variation of the design vector within a defined tolerance, in which the improvement of wheel transition behaviour is observed for various wheel profiles under various track alignments.

Additionally, the study shows that the vertical distance between the top of the wing rail and the nose rail at the transition area, especially at the impact location, is a key factor influencing the dynamic wheel transition behaviour, which in combination with the cross-sectional shape of the nose rail, determines the impact location and the level of impact.

The proposed methodology can be applied both for new crossing designs and the grinding/welding maintenance of existing crossings. For a more specific application case, the parameters of the vehicle–track system can be tuned accordingly. The uncertainty of the vehicle and/or track condition can also be specified by considering the most potential variations of the system.

References

[1] Markine VL, Shevtsov IY. Experimental study on crossing nose damage of railway turnouts in the Netherlands. Proceedings of the Fourteenth International Conference on Civil, Structural and Environmental Engineering Computing (CC2013), paper 37; 2013 September 3–6; Cagliari, Sardinia, Italy.

[2] Wan C, Markine VL, Shevtsov IY. Analysis of train/turnout vertical interaction using a fast numerical model and validation of that model. Proc Instn Mech Eng Part F: J Rail Rapid Transit. 2014;228(7):730–743.

[3] Wan C, Markine VL, Shevtsov IY. Improvement of vehicle-turnout interaction by optimising the shape of crossing nose. Veh Syst Dyn. 2014;52(11):1517–1540.

[4] Pålsson BA. Optimization of railway crossing geometry considering a representative set of wheel profiles. Veh Syst Dyn. 2015;53(2):274–301.

[5] Ben-Tal A, Nemirovski A. Robust optimization – methodology and applications. Math Program. 2002;92(3):453–480.

[6] Mavris DN, Bandte O, DeLaurentis DA. Robust design simulation: a probabilistic approach to multidisciplinary design. J Aircraft. 1999;36(1):298–307.

[7] Ben-Tal A, El-Ghaoui L, Nemirovski A. Robust optimization. Princeton: Princeton University Press; 2009. ISBN: 9781400831050.

[8] Lee KH, Park GJ. Robust optimization considering tolerances of design variables. Comput Struct. 2001;79(1):77–86.

[9] Lönn D, Fyllingen Ø, Nilssona L. An approach to robust optimisation of impact problems using random samples and meta-modelling. Int J Impact Eng. 2010;37(6):723–734.

[10] Diez M, Peri D. Robust optimization for ship conceptual design. Ocean Eng. 2010;37(11–12): 966–977.

[11] Stocki R, Szolc T, Tauzowski P, Knabel J. Robust design optimization of the vibrating rotor-shaft system subjected to selected dynamic constraints. Mech Syst Signal Process. 2012;29:34–44.

[12] Wan C, Markine VL. Parametric study of the wheel transition behaviour at crossings. Veh Syst Dyn. 2015;53(12):1876–1901.

[13] Markine VL. Optimization of the dynamic behaviour of mechanical systems [dissertation]. TU Delft: Shaker Publishing BV; 1999. ISBN 90-423-0069-8.

[14] Toropov VV. Simulation approach to structural optimization. Struct Optim. 1989;1(1):37–46.

[15] Toropov VV. Multipoint approximation method for structural optimization problems with noisy function values. In: Marti, K., Kall P, editors. Stochastic programming: numerical techniques and engineering applications. Lecture Notes in Economics and Mathematical Systems. 1995;423:109–122. Berlin: Springer-Verlag.
[16] Markine VL, Toropov VV. Use of high-and low-fidelity models in approximations for design optimization. Paper presented at the 9th AIAA/ISSMO Symposium on Multidisciplinary Analysis and Optimization; 2002 September 4–6; Atlanta, Georgia, USA.
[17] Wan C, Markine VL, Shevtsov IY. Optimisation of the elastic track properties of turnout crossings. Proc Inst Mech Eng Part F: J Rail Rapid Transit. 2016;230(2):360–373.
[18] Kresselmeier G, Steinhauser R. Systematic control design by optimizing a vector performance index. Proceedings of IFAC Symposium on Computer Aided Design of Control Systems; 1979; Zurich, Switzerland.
[19] Wrenn GA. An indirect method for numerical optimisation using the Kreisselmeier–Steinhauser function. NASA Contractor Report 4220; 1989.
[20] Bertsimas D, Brown DB, Caramanis C. Theory and applications of robust optimization. SIAM Rev. 2011;53:150–168.
[21] Agarwal H. Reliability-based design optimization: formulations and methodologies [dissertation]. Notre Dame: Dept. Mech. Eng., University of Notre Dame; 2004.
[22] Deb K, Gupta S, Daum D, Branke J, Mall AK, Padmanabhan D. Reliability-based optimization using evolutionary algorithms. IEEE Transactions on Evolutionary Computation; 2009 May 13, Institute of Electrical and Electronics Engineers; 1054–1074.
[23] Koch PN. Probabilistic design: optimizing for six sigma quality. In AIAA 43rd AIAA/ASME/ASCE/AHS Structures, Structural Dynamics, and Materials Conference, 4th AIAA Non-Deterministic Approaches Forum, Paper Number AIAA–2002–1471; 2002 April 22–25; Denver, Colorado.

Appendix

Table A1. Track properties used in the simulations.

Track components		Stiffness (MN/m)	Damping (kNs/m)
Rail pad	Vertical	1420	34
	Lateral	280	58
	Roll	360	390
Ballast	Vertical	120	48
	Lateral	120	40
	Roll	130	290